Crystalline splitting of *d* orbitals in two-dimensional regular optical lattices

Hua Chen[1,*] and X. C. Xie[2,3,4]

[1]*Department of Physics, Zhejiang Normal University, Jinhua 321004, China*

[2]*International Center for Quantum Materials, School of Physics, Peking University, Beijing 100871, China*

[3]*Collaborative Innovation Center of Quantum Matter, Beijing 100871, China*

[4]*CAS Center for Excellence in Topological Quantum Computation, University of Chinese Academy of Sciences, Beijing 100190, China*

(Received 31 July 2018; published 7 November 2018)

In solids, crystal field splitting refers to the lifting of atomic orbital degeneracy by the surrounding ions through the static electric field. Similarly, we show that the degenerated *d* orbitals, which were derived in the harmonic oscillator approximation, are split into a low-lying $d_{x^2+y^2}$ singlet and a $d_{x^2-y^2/xy}$ doublet by the high-order Taylor polynomials of triangular optical potential. The low-energy effective theory of the orbital Mott insulator at 2/3 filling is generically described by the Heisenberg-compass model, where the antiferro-orbital exchange interactions of compass type depend on the bond orientation and are geometrically frustrated in the triangular lattice. While, for the square optical lattice, the degenerated *d* orbitals are split into a different multiplet structure, i.e., a low-lying $d_{x^2\pm y^2}$ doublet and a d_{xy} singlet, which has its physical origin in the C_{4v} point group symmetry of square optical potential. Our results build a bridge between ultracold atom systems and solid-state systems for the investigation of *d*-orbital physics.

DOI: 10.1103/PhysRevA.98.053611

I. INTRODUCTION

In transition metal oxides, the degenerated *d* orbitals are split into a set of orbital multiplets, typically a t_{2g} triplet and a e_g doublet for the cubic perovskite structure, by the surrounding oxygen anions through the crystalline electric field, accompanied by the breaking of the full spherical symmetry of a free atom [1,2]. Hence, the key feature of *d* orbitals in solids is that both the orbital degeneracy and orientational anisotropy are governed by the finite point group symmetry of solids. The crystal structure is reflected in the orbital multiplets and is the origin of various interesting phenomena, covering metal-insulator transitions [3], superconductivity [4–8], and colossal magnetoresistance [9–11].

More recently, the forefront of experimental research has focused on the Kitaev material α-$RuCl_3$, in which the relativistic pseudospin-1/2 states arise from the delicate balance of the crystalline electric field, spin-orbit coupling, and strong correlation [12,13]. This material exhibits strongly anisotropic pseudospin exchange interactions originated from the bond-directional nature of *d* orbitals via spin-orbital entanglement, and shows the increasing experimental evidence in supporting the celebrated Kitaev spin-liquid physics [14–18].

Ultracold atom gases offer highly controllable platforms for the quantum simulations of artificial solids in optical lattices, which have served successfully as a complementary setup to solid-state systems during the past decade [19]. As a paradigmatic example, the *p*-orbital physics in optical lattices attracts intensive research interest for the orbital degree of freedom [20–22]. Interesting many-body phenomena were predicted including unconventional Bose-Einstein condensation [23–25], supersolid phase [26], stripe ordering [27], Wigner crystallization [28], and orbital ordering in Mott insulators [29–31]. Importantly, the chiral $p_x \pm ip_y$ superfluidity has been successfully observed in recent experiments [32–34]. However, the *p* orbitals are essentially different from the *d* orbitals for both orbital degeneracy and orientational anisotropy.

Particularly exciting is the recent experimental advance in the observation of *d* orbitals in optical lattices [35–38], which makes an important step toward genuinely emulating *d*-orbital physics of solid-state systems. Here we report that the degeneracy of *d* orbitals, which was predicted in the harmonic oscillator (HO) approximation, is partly removed by the high-order Taylor polynomials (HOTPs) of optical potential in both triangular and square optical lattices. In the triangular lattice, the orbital Mott insulator is further studied based on the remaining degeneracy between $d_{x^2-y^2}$ and d_{xy} orbitals. The corresponding orbital exchange Hamiltonian is generically described by the Heisenberg-compass model, where the anisotropic compass interactions have roots in the orbital orientational anisotropy and are geometrically frustrated. For the square lattice, in particular, we have derived a selection rule on the orbital angular momentum and show that the geometry of a square optical lattice plays a crucial role in determining the orbital multiplets.

II. TRIANGULAR OPTICAL LATTICE

The triangular optical potential has been theoretically proposed [39,40] and experimentally realized [41–43] using three linearly polarized laser beams. It is mathematically described by $V_\triangle(\boldsymbol{r}) \equiv -V\sum_{i=1}^{3}\cos(\boldsymbol{b}_i\cdot\boldsymbol{r})$, where the reciprocal lattice vectors $\boldsymbol{b}_1 = \frac{2\pi}{a}(\hat{x} + \frac{1}{\sqrt{3}}\hat{y})$, $\boldsymbol{b}_2 = \frac{2\pi}{a}(-\hat{x} + \frac{1}{\sqrt{3}}\hat{y})$, and $\boldsymbol{b}_3 =$

*hwachanphy@zjnu.edu.cn

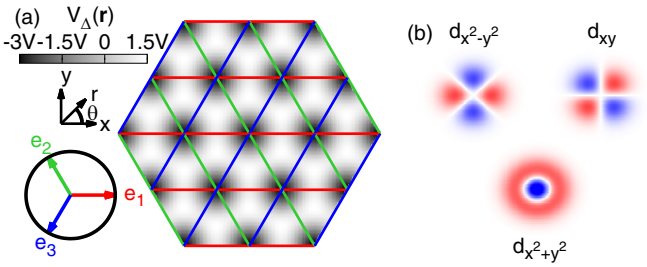

FIG. 1. (a) Grey map of the triangular optical potential $V_\triangle(\boldsymbol{r})$. $\{\boldsymbol{e}_1, \boldsymbol{e}_2, \boldsymbol{e}_3\}$ are the bond vectors of triangular lattice. (b) Structure of partially lifted degeneracy of d-orbital multiplets in the triangular optical lattice.

$-\frac{4\pi}{\sqrt{3}a}\hat{y}$ with a the lattice spacing. Figure 1(a) plots the periodic landscape of optical potential $V_\triangle(\boldsymbol{r})$, the spatial modulation of which realizes the triangular lattice. Since the lattice is invariant under primitive translations of bond vectors $\{\boldsymbol{e}_1, \boldsymbol{e}_2, \boldsymbol{e}_3\}$, we will focus on the lattice site at the origin of coordinates to simplify the discussion. Switching to polar coordinates (r, θ), the optical potential can be expressed in terms of Bessel functions of the first kind via the Jacobi-Anger expansion,

$$V_\triangle(\boldsymbol{r}) = \sum_{\ell=-\infty}^{+\infty} V_\triangle^\ell(r)\exp[6i\ell\theta], \quad V_\triangle^\ell(r) \equiv -3V J_{6\ell}\frac{4\bar{r}}{\sqrt{3}}, \tag{1}$$

with the dimensionless radial distance $\bar{r} \equiv \pi r/a$. A Taylor series expansion of the isotropic component $V_\triangle^{\ell=0} = -3V + 4V\bar{r}^2 + O(\bar{r}^4)$ in Eq. (1) yields a two-dimensional (2D) harmonic trapping of frequency $\omega = \sqrt{8\pi^2 V/Ma^2}$ (M is the mass of trapped atoms). In the deep lattice limit, the Wannier functions in the optical potential $V_\triangle(\boldsymbol{r})$ are well approximated by the corresponding eigenfunctions of HO [24,25].

Due to the isotropic nature of the 2D HO, the eigenfunctions have simultaneous eigenstates with the z-axis angular momentum operator $L_z = -i\hbar\partial_\theta$ and thus can be written in the axial states

$$\Psi_{[n,m]}(\boldsymbol{r}) \equiv R_{[n,m]}(r)\exp[im\theta],$$

with n and m labeling the quanta of the 2D HO and z-axis angular momentum, respectively (see Appendix A for details). The explicit forms of eigenfunctions $\Psi_{[n,m]}(\boldsymbol{r})$ for $n = 2$, which we will refer to as d orbitals hereafter, are listed in Table I.

TABLE I. d-orbital wave functions $\Psi_{[n=2,m]}(\boldsymbol{r})$ of the 2D isotropic harmonic oscillator of frequency ω with $\beta \equiv \sqrt{M\omega/\hbar}$.

n	m	$\Psi_{[n,m]}(\boldsymbol{r}) \equiv R_{[n,m]}(r)\exp[im\theta]$
2	$+2$	$\Psi_{[2,+2]}(\boldsymbol{r}) = \frac{\beta^3}{\sqrt{2\pi}}r^2\exp\left[-\frac{\beta^2 r^2}{2}\right]\exp[+2i\theta]$
	0	$\Psi_{[2,0]}(\boldsymbol{r}) = \frac{\beta}{\sqrt{\pi}}\left[(\beta r)^2 - 1\right]\exp\left[-\frac{\beta^2 r^2}{2}\right]$
	-2	$\Psi_{[2,-2]}(\boldsymbol{r}) = \frac{\beta^3}{\sqrt{2\pi}}r^2\exp\left[-\frac{\beta^2 r^2}{2}\right]\exp[-2i\theta]$

Next, we will show that the high-order polynomials in the Taylor series expansion of isotropic potential $V_\triangle^{\ell=0}(r)$ will further lift the degeneracy of the d-orbital complex. To proceed, we expand field operators in the d-orbital Wannier basis and obtain the second quantization form of HOTPs in $V_\triangle(\boldsymbol{r})$ in Eq. (1)

$$\mathscr{H}_\triangle = \sum_{m_1 m_2}\sum_{\ell=-\infty}^{+\infty}\langle\Psi_{[2,m_1]}|\triangle^\ell|\Psi_{[2,m_2]}\rangle\hat{\Psi}^\dagger_{[2,m_1]}\hat{\Psi}_{[2,m_2]}, \tag{2}$$

where the HOTPs $\triangle^\ell(\boldsymbol{r}) \equiv V_\triangle^\ell(r)\exp[6i\ell\theta] + (3V - 4V\bar{r}^2)\delta_{\ell,0}$ and $\hat{\Psi}^\dagger_{[2,m]}$ ($\hat{\Psi}_{[2,m]}$) creates (annihilates) an atom in the state $\Psi_{[n=2,m]}$. It is easy to verify that the matrix elements of anisotropic potential $\triangle^{\ell\neq 0}_{m_1 m_2} \equiv \langle\Psi_{[2,m_1]}|\triangle^\ell|\Psi_{[2,m_2]}\rangle$ have no contributions because of the vanishing integrals of azimuthal parts over polar angle θ. While, for the isotropic case $\ell = 0$, the matrix $\triangle^{\ell=0}_{m_1 m_2}$ has nonvanishing diagonal elements

$$\{\triangle^{\ell=0}_{\pm2,\pm2}, \triangle^{\ell=0}_{0,0}\} = -\frac{E_R}{12}\sum_{l=0}^{\infty}\left(-\frac{1}{3}\sqrt{\frac{E_R}{2V}}\right)^l\frac{1}{(l+2)!} \times \{l^2 + 7l + 12,\ 2l^2 + 10l + 14\},$$

with the recoil energy $E_R \equiv 4\hbar^2\pi^2/Ma^2$. The axial states $\Psi_{[n=2,m=\pm2]}$ have the identical correction on their energy levels by the HOTPs $\triangle^{\ell=0}(\boldsymbol{r})$. The reason can be traced back to the fact that their eigenfunctions share the same radial function, as listed in Table I. A unitary transformation $\Psi_{[n=2,m=\pm2]} \equiv (d_{x^2-y^2} \pm id_{xy})/\sqrt{2}$ and $\Psi_{[n=2,m=0]} \equiv d_{x^2+y^2}$ [44], followed by an irrelevant energy shift of $\triangle^{\ell=0}_{0,0}$, cast $\mathscr{H}_\triangle$ in Eq. (2) into a concrete form

$$\mathscr{H}_\triangle = \triangle(d^\dagger_{x^2-y^2}d_{x^2-y^2} + d^\dagger_{xy}d_{xy}), \tag{3}$$

with $\triangle \equiv \triangle^{\ell=0}_{\pm2,\pm2} - \triangle^{\ell=0}_{0,0} = \frac{E_R}{12}\exp\left[-\frac{1}{3}\sqrt{\frac{E_R}{V}}\right]$ describing the energy splitting between $d_{x^2-y^2/xy}$ and $d_{x^2-y^2}$ orbitals. In the deep lattice limit, $V \gg E_R$, the energy splitting $\triangle$ saturates at $E_R/12$, and the d-orbital complex is well separated from the s and $p_{x,y}$ orbitals in energy, primarily by the HO frequency $\hbar\omega = \sqrt{2VE_R}$, indicating the validity of first-order perturbation treatment above. As is summarized in Fig. 1(b), the d-orbital complex splits into a low-lying $d_{x^2+y^2}$ singlet and a $d_{x^2-y^2/xy}$ doublet, which is analogous to the crystalline electric field splitting in solid-state physics [45]. When a d-orbital ion is embedded in a solid, the full fivefold degeneracy of hydrogen-like d orbitals, which is protected by the spherical symmetry of a free atom, is lifted by the charged neighboring ions through the crystal field potential. While the splitting of a d-orbital complex in the triangular optical lattice is rooted in the different radial functions between $d_{x^2-y^2/xy}$ and $d_{x^2-y^2}$ orbitals through the isotropic high-order optical potential $\triangle^{\ell=0}(\boldsymbol{r})$. We will show that the anisotropic optical potential can also contribute to the degeneracy lifting in a different manner, see discussions on the square optical lattice later.

It is then interesting to explore the interplay between the geometrical frustration of a triangular lattice and the quantum fluctuation, which is enhanced by the remaining degeneracy of $d_{x^2-y^2}$ and d_{xy} orbitals. The pioneering works have studied $p_{x,y}$-orbital Mott insulators with spinless fermions and

found various exotic orbital orderings in the classical ground states [29,30]. To this end, it is necessary to carry out a strong coupling study of the correlated d-orbital systems. Let us start with the case that spinless fermions interact with each other through a general central potential $\hat{U}(r)$. The interacting Hamiltonian is constructed in terms of the Haldane pseudopotentials

$$\mathscr{H}_{\rm I} = \sum_m \sum_{i<j} v_m \mathcal{P}_m(ij),$$

where $\mathcal{P}_m(ij)$ is the projection operator which selects out states in which particles i and j have relative angular momentum m [46]. According to the Fermi (Bose) statistics, the many-particle state of fermions (bosons) should be antisymmetric (symmetric) upon interchanging two particles, which requires that m is odd (even). Thus, the pseudopotential set $\{v_m\}$ with odd m provides a complete and unique description of interaction $\hat{U}(r)$ for spinless fermions. For a short-range interaction $\hat{U}(r)$, the leading interaction between d orbitals is described by

$$\mathscr{H}_{\rm I} = U[(\hat{n}_{x^2-y^2} + \hat{n}_{xy})\hat{n}_{x^2+y^2} + 2\hat{n}_{x^2-y^2}\hat{n}_{xy}], \qquad (4)$$

where $U \equiv 3v/16\pi$ and the Haldane pseudopotentials $v_{\pm 1} \equiv v$ are the short-range components of $\hat{U}(r)$ in active channels $m = \pm 1$ (see Appendix B for details). The interactions between the d orbitals and the low-lying s and $p_{x,y}$ orbitals cannot lift the remaining degeneracy of d orbitals in Eq. (3), which is protected by the continuous rotation symmetry. The well-separated s and $p_{x,y}$ orbitals are reminiscent of the closed shells in solid-state systems and remain inactive at low energy scales. Interestingly, the d orbitals can be prepared by the direct transfer between even-parity orbitals $s \to d$ with the fidelities as high as 97–99% in recent experiments [37,38]. Therefore, in the following, we shall only consider the interaction between d orbitals. For the case that the d orbitals are partially occupied by n spinless fermions, we will refer to it as a d^n configuration. Including the crystalline splitting $\mathscr{H}_\triangle$ in Eq. (3) and the on-site interaction $\mathscr{H}_{\rm I}$ in Eq. (4), the ground state of the d^2 configuration is an orbital doublet with one fermion occupying the low-lying $d_{x^2+y^2}$ orbital and the other one occupying either the $d_{x^2-y^2}$ or d_{xy} orbital, and simply inherits the partially degeneracy of the d-orbital complex.

It is convenient for later discussions to define the pseudospin operators $\{\tau^+, \tau^-\} \equiv \{d^\dagger_{x^2-y^2} d_{xy} \hat{n}_{x^2+y^2}, d^\dagger_{xy} d_{x^2-y^2} \hat{n}_{x^2+y^2}\}$, which flip the states of orbital doublet. The z component of the pseudospin $\boldsymbol{\tau}$ vector follows through the spin-1/2 angular momentum algebra $\tau^z = [\tau^+, \tau^-]$. In the strongly correlated regime, orbital fluctuation is the remaining low-energy degree of freedom. Therefore, the effective model is captured by the orbital superexchange interactions between sites i and j, which arise from the virtual charge excitations $(d^2)_i(d^2)_j \rightleftharpoons (d^3)_i(d^1)_j$ through the hopping process $t_{\mu\nu} d^\dagger_{i\mu} d_{j\nu}$ $(\mu, \nu = x^2-y^2, xy, x^2+y^2)$. Employing the second-order perturbation theory in Ref. [47], we derive the effective Hamiltonian in Appendix C. It is generically described by the Heisenberg-compass model $\mathscr{H}^{\rm eff}_\triangle = \mathscr{H}_{\rm H} + \mathscr{H}^{120^\circ}_\triangle$, where the isotropic Heisenberg term $\mathscr{H}_{\rm H} = J_{\rm H} \sum_{i\eta\gamma} \boldsymbol{\tau}_i \cdot \boldsymbol{\tau}_{i+\eta \boldsymbol{e}_\gamma}$ and the anisotropic compass term [48,49]

$$\mathscr{H}^{120^\circ}_\triangle = J_{\rm C} \sum_{i\gamma\eta} \tau^\gamma_i \tau^\gamma_{i+\eta \boldsymbol{e}_\gamma} \qquad (5)$$

with

$$\tau^\gamma = \tau^z \cos[4\theta_\gamma] + \tau^x \sin[4\theta_\gamma],$$
$$\boldsymbol{e}_\gamma = \hat{x}\cos\theta_\gamma + \hat{y}\sin\theta_\gamma,$$
$$\{\theta_1, \theta_2, \theta_3\} = \left\{0, \frac{2\pi}{3}, \frac{4\pi}{3}\right\}, \quad \eta = \pm 1.$$

The superexchange couplings are given by

$$\{J_{\rm H}, J_{\rm C}\} = \{t_\pi t_\sigma / U, (t_\sigma - t_\pi)^2/2U\}$$

with t_π (t_σ) denoting the intraorbital $\pi(\sigma)$-bonding state of the d_{xy} $(d_{x^2-y^2})$ orbital.

It is worth noting that the π-bonding axis lies in the nodal plane of the d_{xy} orbital. As a result, the π bonding is typically much weaker than the σ bonding, and the corresponding antiferro-orbital compass interaction dominates over the ferro-orbital Heisenberg interaction ($J_{\rm H} < 0$ is due to the opposite sign of t_π and t_σ). This is reminiscent of the Heisenberg-Kitaev model in the afore-mentioned Kitaev material α-$RuCl_3$ with the dominant Kitaev coupling [12,13]. Solving the quantum Heisenberg-compass model remains a challenging problem. Nevertheless, it is instructive to first determine the ground state of the dominant part, i.e., the quantum compass model [49], for understanding the phase diagram of the quantum Heisenberg-compass model. The particularity of the quantum compass model $\mathscr{H}^{120^\circ}_\triangle$ in Eq. (5) is that along the bond vector $\pm\boldsymbol{e}_\gamma$ $(\gamma = 1, 2, 3)$ the exchange interaction involves the pseudospin τ^γ of two sites connected by the bond, and the pseudospin components $\tau^{1,2,3}$ intersect in the zx plane at an effective angle of 120°. The quantum 120° model is first introduced as an effective model for perovskite e_g orbital systems [50], which is closely related to the well-known quantum compass model [51]. Apparently, it is impossible to minimize the antiferro-orbital interactions for all three bonds on an elementary triangle simultaneously due to the geometrical frustration. In this case, exotic quantum states are usually promoted by the geometrical frustration via spontaneous symmetry breaking.

To capture the quantum fluctuations, we resort to Lanczos exact diagonalization on finite-size clusters. As illustrated in Figs. 2(a) and 2(b), we first employ the clusters with 60° equilateral parallelograms to avoid the cluster shape dependence of the results [52]. The corresponding energy spectra are carefully analyzed by extracting the momentum of each eigenstate. One key signature in the spectrum of a 12-site cluster is that several low-lying states are well separated from the excited states by a clear gap. The energies of these low-lying states are much lower than the ground-state energy of the 21-site cluster. It is well accepted that the quantum counterpart of the classical ground state is a coherent superposition of low-lying eigenstates, which are dubbed as quasidegenerate joint states (QDJSs) [53,54]. As shown in Fig. 2(c), further studies on the 16-site cluster confirm that the energy spread of QDJSs decreases upon increasing the size of the cluster. Importantly, the QDJSs involve three degenerate states at the M points of the hexagonal Brillouin zone, which provides strong evidence

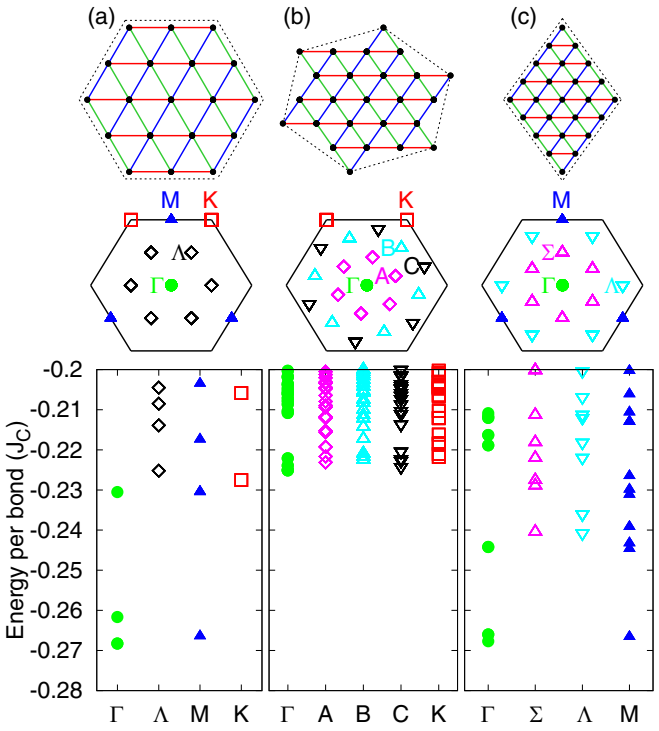

FIG. 2. Low-energy spectra (bottom panel) of quantum 120° compass model on the finite-size clusters of (a) 12 sites, (b) 21 sites, and (c) 16 sites with exchange couplings $(J_C, J_H) = (1, 0)$. The x axis labels the momenta of many-particle states, which are marked in the hexagonal Brillouin zone (middle panel). The corresponding samples of finite-size clusters with periodic boundary conditions (black dashed lines) are shown in the top panel.

that the macroscopic symmetry-breaking state is of columnar type.

Interestingly, the energies of QDJSs are close to the energy of the classical columnar state, $-0.25J_C$ per bond. This classical state is also proposed as the ground state of $p_{x,y}$-orbital Mott insulators in Ref. [30]. While, in the Heisenberg limit ($J_H < 0$, $J_C = 0$), the ferro-orbital exchange favors parallel alignments of nearest neighbor orbitals along bonds and is thus free of geometrical frustration. The transition between classical columnar phase and ferro-orbital phase occurs at the critical value $J_C = -8J_H/3$, above which the classical columnar state is stabilized. As shown in Fig. 2, the columnar phase is associated with the QDJSs at the Γ and M points of the hexagonal Brillouin zone. The interference between QDJSs at the Γ and M points breaks both the translation symmetry of the triangular lattice and the point group symmetry from C_6 down to C_2 symmetry, which can be distinguished from the ferro-orbital phase. Experimentally, the symmetry breaking can in principle be detected by the time-of-flight interference [55]. It is also noteworthy that the breaking of translation symmetry leads to the enlarged unit cell in the columnar phase. In the time-of-flight noise correlation spectra, the momentum resolved interference spots will be observed at the corresponding reciprocal lattice points in the columnar phase, from which the broken symmetries can be easily identified.

III. SQUARE OPTICAL LATTICE

Next, we turn to the square optical potential $V_\square(\boldsymbol{r}) = -V[\cos(\boldsymbol{b}_1\cdot\boldsymbol{r}) + \cos(\boldsymbol{b}_2\cdot\boldsymbol{r})]$ with the reciprocal lattice vectors $\boldsymbol{b}_1 = \frac{2\pi}{a}\hat{x}$ and $\boldsymbol{b}_2 = \frac{2\pi}{a}\hat{y}$. The Jacobi-Anger expansion of the square optical potential leads to

$$V_\square(\boldsymbol{r}) = \sum_{\ell=-\infty}^{+\infty} V_\square^\ell(r)\exp[4i\ell\theta], \quad V_\square^\ell(r) \equiv -2VJ_{4\ell}\frac{2\pi r}{a}. \tag{6}$$

The curvature at the bottom of isotropic component $V_\square^{\ell=0} = -2V + 2V\pi^2r^2/a^2 + O(r^4)$ in Eq. (6) dictates the HO frequency $\omega = \sqrt{4V\pi^2/Ma^2}$. The high-order correction on the d-orbital complex is then described by

$$\mathscr{H}_\square = \sum_{m_1m_2}\sum_{\ell=-\infty}^{+\infty}\langle\Psi_{[2,m_1]}|\square^\ell|\Psi_{[2,m_2]}\rangle\hat{\Psi}^\dagger_{[2,m_1]}\hat{\Psi}_{[2,m_2]}, \tag{7}$$

where $\square^\ell(\boldsymbol{r}) \equiv V_\square^\ell(r)\exp[4i\ell\theta] + (2V - 2V\pi^2r^2/a^2)\delta_{\ell,0}$. The nonzero diagonal elements in the isotropic channel $\ell = 0$ are given by

$$\{\square^{\ell=0}_{\pm2,\pm2}, \square^{\ell=0}_{0,0}\} = -\frac{E_R}{16}\sum_{l=0}^{\infty}\left(-\frac{1}{4}\sqrt{\frac{E_R}{V}}\right)^l\frac{1}{(l+2)!} \times\{l^2+7l+12,\ 2l^2+10l+14\}.$$

While, for the anisotropic channel $\ell \neq 0$, the integral over the polar angle θ yields a selection rule $m_1 - m_2 = 4\ell$, which has an intuitive meaning from the view of angular momentum conservation: m_1 (m_2) is the angular momentum in the final (initial) state and 4ℓ is supplied by the square optical lattice because it has a fourfold discrete rotational symmetry. The nonvanishing terms, satisfying the selection rule, are explicitly evaluated as

$$\square^{\ell=1}_{+2,-2} = \square^{\ell=-1}_{-2,+2} = \frac{E_R}{16}\exp\left[-\frac{1}{4}\sqrt{\frac{E_R}{V}}\right].$$

The reduction of continuous z-axis rotation symmetry lifts the degeneracy of time-reversal partners $\Psi_{[n=2,m=\pm2]}$ and quenches the orbital momentum. Finally, a little algebra, together with an overall energy shift of $\square^{\ell=0}_{0,0}$, casts $\mathscr{H}_\square$ in Eq. (7) into the form

$$\mathscr{H}_\square = \square(d^\dagger_{xy}d_{xy} - d^\dagger_{x^2-y^2}d_{x^2-y^2} - d^\dagger_{x^2+y^2}d_{x^2+y^2}),$$

with $\square \equiv \frac{E_R}{16}\exp[-\frac{1}{4}\sqrt{\frac{E_R}{V}}]$ describing the energy splitting between $d_{x^2\pm y^2}$ and d_{xy} orbitals. Figure 3(b) depicts the structure of d-orbital multiplets in the square optical lattice. From symmetry aspects, the $\{d_{x^2+y^2}, d_{x^2-y^2}, d_{xy}\}$ orbitals belong to the irreducible representations $\{A_1, B_1, B_2\}$ of C_{4v} point group symmetry, respectively [56]. It is noteworthy that the C_{4v} symmetry is not sufficient to guarantee the degeneracy of the $d_{x^2\pm y^2}$ doublet, which can be lifted in a checkerboard optical potential.

In the d^1 configuration, the ground state is an orbit doublet with one fermion occupying either the $d_{x^2+y^2}$ or $d_{x^2-y^2}$ orbital. In the large-U limit, we next briefly discuss the corresponding low-energy effective model that is constructed based on the ground-state doublet through the virtual charge

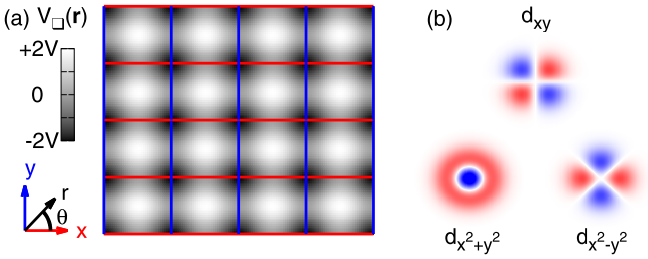

FIG. 3. (a) Grey map of the square optical potential $V_{\square}(\boldsymbol{r})$. (b) Structure of partially lifted degeneracy of d-orbital multiplets in the square optical lattice.

excitations $(d^1)_i(d^1)_j \rightleftharpoons (d^2)_i(d^0)_j$. For the case that the hopping integral $t_{\mu\nu}$ is comparable to the crystalline splitting $\square$, the occupation of the d_{xy} orbital through the crystal-field excitation cannot be neglected. Therefore, the orbital doublet is inadequate for constructing the low-energy effective model for this case. In contrast, the crystal-field excitation in the d^2 configuration is suppressed by the interaction U in the triangular lattice. While for the case $t_{\mu\nu} \ll \square$, we follow the procedure described in Appendix C. It is straightforward to show that the leading-order Hamiltonian takes the form

$$\mathscr{H}_{\square}^{\text{eff}} = J_z \sum_{\langle ij \rangle} \tau_i^z \tau_j^z \tag{8}$$

with the antiferro-orbital Ising coupling $J_z = 2t_\sigma^2/U$ and the pseudospin $\tau^z = (d^\dagger_{x^2+y^2} d_{x^2+y^2} - d^\dagger_{x^2-y^2} d_{x^2-y^2})/2$. The antiferro-orbital coupling favors Néel ordering in the square lattice. Due to the extra constraint $t_\sigma \ll \square$, it may require extremely low temperatures to experimentally detect the orbital ordering through the time-of-flight interference.

IV. SUMMARY

In conclusion, we have shown that the degeneracy of d orbitals is lifted in both triangular and square optical lattices by a perturbative treatment. In particular, the selection rule is invoked in determining the symmetry reduction from the z-axis rotation symmetry of a harmonic oscillator approximation to the discrete point group symmetry of optical potential. We emphasize that our theory can be easily generalized to the superstructured optical lattices, such as a checkerboard lattice, and is capable of predicting the orbital degeneracy from symmetry aspects. Therefore our theory has potential applications in the quantum material design of optical lattices. Our work shall attract more experimental efforts in engineering d orbitals, and may open fascinating new ground for the quantum simulation of strongly correlated d-orbital physics in optical lattices.

ACKNOWLEDGMENTS

We thank Haiwen Liu, Xiongjun Liu, Congjun Wu, and Hongyu Yang for helpful discussions. This work is supported by the National Natural Science Foundation of China under Grants No. 11704338, No. 11534001, and No. 11504008, and the National Basic Research Program of China under Grant No. 2015CB921102.

APPENDIX A: ALGEBRAIC SOLUTIONS OF AN ISOTROPIC TWO-DIMENSIONAL HARMONIC OSCILLATOR

We will derive the algebraic solutions of an isotropic 2D harmonic oscillator that is described by the following Hamiltonian:

$$\mathscr{H}_{\text{HO}} = \frac{\hat{\boldsymbol{p}}^2}{2M} + \frac{1}{2}M\omega^2 r^2,$$

where M is the mass of atoms trapped in the quantum well and ω is the harmonic frequency. The isotropic 2D harmonic oscillator can split into two 1D uncoupled oscillators in $\mu = x, y$ directions

$$\mathscr{H}_\mu = \frac{\hat{p}_\mu^2}{2M} + \frac{1}{2}M\omega^2\mu^2.$$

Let us first introduce the lowering and raising operators for the 1D harmonic oscillators

$$a_\mu = \frac{1}{\sqrt{2}}\left(\beta\mu + i\frac{\hat{p}_\mu}{\beta\hbar}\right),$$
$$a_\mu^\dagger = \frac{1}{\sqrt{2}}\left(\beta\mu - i\frac{\hat{p}_\mu}{\beta\hbar}\right),$$

with $\beta \equiv \sqrt{\frac{M\omega}{\hbar}}$. In terms of number operators $\hat{n}_\mu = a_\mu^\dagger a_\mu$, the Hamiltonian of the 2D oscillator can be rewritten as $\mathscr{H}_{\text{HO}} = \hbar\omega(\hat{n}_x + \hat{n}_y + 1)$. Thus, the eigenfunctions $\psi_{[n_x,n_y]}(\boldsymbol{r})$ of the 2D oscillator, corresponding to the energy $E = \hbar\omega(n_x + n_y + 1)$, are characterized by 1D harmonic oscillator quanta n_μ in $\mu = x, y$ directions. Since the isotropic 2D harmonic oscillator is invariant under rotation about the z axis, the Hamiltonian $\mathscr{H}_{\text{HO}}$ should commute with the operator $\hat{L}_z = x\hat{p}_y - y\hat{p}_x$ of infinitesimal rotation about the z axis, i.e., the z-component angular momentum operator. In the following, we shall seek a basis of eigenfunctions common to both $\mathscr{H}_{\text{HO}}$ and $\hat{L}_z$. To take better advantage of the continuous rotation symmetry, we introduce the chiral operators as follows:

$$a_\pm^\dagger = \frac{1}{\sqrt{2}}(a_x^\dagger \pm i a_y^\dagger).$$

It is easy to verify that the only nonzero commutators between chiral operators are $[a_+, a_+^\dagger] = [a_-, a_-^\dagger] = 1$. The corresponding number operators $\hat{n}_\pm = a_\pm^\dagger a_\pm$ count the number of right(+) and left(−) circular quanta. With this definition, the Hamiltonian can be rewritten as $\mathscr{H}_{\text{HO}} = \hbar\omega(\hat{n}_+ + \hat{n}_- + 1) \equiv \hbar\omega(\hat{n} + 1)$ with $\hat{n} \equiv \hat{n}_+ + \hat{n}_-$ being the total quanta operator. In addition, the z-component angular momentum operator can also be rewritten as $\hat{L}_z = \hbar(\hat{n}_+ - \hat{n}_-) \equiv \hbar\hat{m}$ with $\hat{m} \equiv \hat{n}_+ - \hat{n}_-$. Therefore, the eigenfunctions of $\mathscr{H}_{\text{HO}}$ can be characterized by either $[n_+, n_-]$ or $[n, m]$. The ground state $\Psi_{[n=n_++n_-=0, m=n_+-n_-=0]}(\boldsymbol{r})$ contains no right $(n_+ = 0)$ and left $(n_- = 0)$ circular quanta and is identical to $\psi_{[n_x=0,n_y=0]}(\boldsymbol{r})$ up to a phase. The eigenfunctions of excited states can be evaluated by applying the chiral operators $a_\pm^\dagger$ to the ground state

$$\Psi_{[n=n_++n_-, m=n_+-n_-]}(\boldsymbol{r}) = \frac{(a_+^\dagger)^{n_+}(a_-^\dagger)^{n_-}}{\sqrt{n_+!n_-!}}\Psi_{[0,0]}(\boldsymbol{r}).$$

TABLE II. Eigenfunctions $\Psi_{[n,m]}(\boldsymbol{r})$ of the 2D isotropic harmonic oscillator for $n = \{0, 1, 2\}$.

$n \equiv n_+ + n_-$	$m \equiv n_+ - n_-$	n_+	n_-	$\Psi_{[n,m]}(\boldsymbol{r}) \equiv R_{[n,m]}(r)\exp[im\theta]$
$n=0$	$m=0$	$n_+=0$	$n_-=0$	$\Psi_{[0,0]}(\boldsymbol{r}) = \frac{\beta}{\sqrt{\pi}}\exp\left[-\frac{\beta^2 r^2}{2}\right]$
$n=1$	$m=+1$	$n_+=1$	$n_-=0$	$\Psi_{[1,+1]}(\boldsymbol{r}) = \frac{\beta^2}{\sqrt{\pi}} r\exp\left[-\frac{\beta^2 r^2}{2}\right]\exp[+i\theta]$
	$m=-1$	$n_+=0$	$n_-=1$	$\Psi_{[1,-1]}(\boldsymbol{r}) = \frac{\beta^2}{\sqrt{\pi}} r\exp\left[-\frac{\beta^2 r^2}{2}\right]\exp[-i\theta]$
$n=2$	$m=+2$	$n_+=2$	$n_-=0$	$\Psi_{[2,+2]}(\boldsymbol{r}) = \frac{\beta^3}{\sqrt{2\pi}} r^2\exp\left[-\frac{\beta^2 r^2}{2}\right]\exp[+2i\theta]$
	$m=0$	$n_+=1$	$n_-=1$	$\Psi_{[2,0]}(\boldsymbol{r}) = \frac{\beta}{\sqrt{\pi}}\left[(\beta r)^2 - 1\right]\exp\left[-\frac{\beta^2 r^2}{2}\right]$
	$m=-2$	$n_+=0$	$n_-=2$	$\Psi_{[2,-2]}(\boldsymbol{r}) = \frac{\beta^3}{\sqrt{2\pi}} r^2\exp\left[-\frac{\beta^2 r^2}{2}\right]\exp[-2i\theta]$

The explicit forms of eigenfunctions $\Psi_{[n,m]}(\boldsymbol{r})$ for $n = \{0, 1, 2\}$ are listed in Table II.

APPENDIX B: HALDANE PSEUDOPOTENTIAL DESCRIPTIONS OF INTERACTING HAMILTONIAN

The central interaction potential $\hat{U}(r)$ that depends only on the relative coordinate r between particle pairs can be described by a set of Haldane pseudopotentials v_m [46]. The potentials v_m are obtained from the decomposition of two-particle states into the states with relative angular momentum m. According to the Fermi (Bose) statistics, the many-particle state of fermions (bosons) upon interchanging two particles is antisymmetric (symmetric), which requires that m is odd (even). For the present case of spinless fermions with short-range interaction, we restrict the relative motion of two-particle states in the lowest odd angular momentum $m = \pm 1$, corresponding to the p-wave channel. Specifically, the two-particle state is factorized into two decoupled wave functions that describe the center-of-mass $[\boldsymbol{r}_+ \equiv \frac{1}{2}(\boldsymbol{r}_1 + \boldsymbol{r}_2)]$ motion and the relative $(\boldsymbol{r}_- = \boldsymbol{r}_1 - \boldsymbol{r}_2)$ motion

$$\begin{aligned}&\Psi_{n=2,m_1}(\boldsymbol{r}_1)\Psi_{n=2,m_2}(\boldsymbol{r}_2)\\ &\approx r_-\exp\left[-\beta^2\left(r_+^2+\frac{r_-^2}{4}\right)\right]\left\{\chi^+_{m_1m_2}(\boldsymbol{r}_+)\exp[i\theta_-]\right.\\ &\left.+\chi^-_{m_1m_2}(\boldsymbol{r}_+)\exp[-i\theta_-]\right\},\end{aligned}\tag{B1}$$

where $\chi^{\pm}_{m_1m_2}(\boldsymbol{r}_+)$ are listed in Table III. In Eq. (B1), we neglect the high-order terms in r_- and keep the linear terms in the brace, which corresponds to the short-range components of the interaction. Such an approximation is valid when the effective range of interaction is much shorter than the characteristic length of the 2D harmonic oscillator. It is straightforward to show that the interacting Hamiltonian takes the following form:

$$\mathscr{H}_{\rm I} = \tfrac{1}{2}U_{m_1m_2m_3m_4}d^\dagger_{m_1}d^\dagger_{m_2}d_{m_3}d_{m_4}$$

with the interaction matrix

$$\begin{aligned}U_{m_1m_2m_3m_4} \equiv \int d^2\boldsymbol{r}_+\frac{1}{\beta^4}\left[v_{+1}\chi^{+*}_{m_2m_1}(\boldsymbol{r}_+)\chi^+_{m_3m_4}(\boldsymbol{r}_+)\right.\\ \left.+\,v_{-1}\chi^{-*}_{m_2m_1}(\boldsymbol{r}_+)\chi^-_{m_3m_4}(\boldsymbol{r}_+)\right]\exp[-2\beta^2r_+^2],\end{aligned}\tag{B2}$$

and the Haldane pseudopotentials $v_{\pm1} = \beta^4\int d^2\boldsymbol{r}_-r_-\exp[-\beta^2\frac{r_-^2}{4}]\hat{U}(r_-)r_-\exp[-\beta^2\frac{r_-^2}{4}] \equiv v$. A little algebra on the integral of Eq. (B2) over the center-of-mass coordinates $\boldsymbol{r}_+$ and a unitary basis transformation lead to the following Hamiltonian:

$$\mathscr{H}_{\rm I} = \frac{3v}{16\pi}[(\hat{n}_{x^2-y^2}+\hat{n}_{xy})\hat{n}_{x^2+y^2} + 2\hat{n}_{x^2-y^2}\hat{n}_{xy}].$$

TABLE III. Wave functions $\chi^{\pm}_{m_1m_2}(\boldsymbol{r}_+)$ describe the center-of-mass motion of two-particle states in Eq. (B1).

	$\chi^+_{m_1m_2}(\boldsymbol{r}_+)$		
	$m_2=-2$	$m_2=0$	$m_2=+2$
$m_1=-2$	0	$-\frac{\beta^6}{2\sqrt{2\pi}}r_+^3\exp[-3i\theta_+]$	$-\frac{\beta^6}{2\pi}r_+^3\exp[-i\theta_+]$
$m_1=0$	$\frac{\beta^6}{2\sqrt{2\pi}}r_+^3\exp[-3i\theta_+]$	0	$-\frac{\beta^4}{\sqrt{2\pi}}r_+\left(\frac{1}{2}\beta^2r_+^2-1\right)\exp[i\theta_+]$
$m_1=+2$	$\frac{\beta^6}{2\pi}r_+^3\exp[-i\theta_+]$	$\frac{\beta^4}{\sqrt{2\pi}}r_+\left(\frac{1}{2}\beta^2r_+^2-1\right)\exp[i\theta_+]$	0
	$\chi^-_{m_1m_2}(\boldsymbol{r}_+)$		
	$m_2=-2$	$m_2=0$	$m_2=+2$
$m_1=-2$	0	$\frac{\beta^4}{\sqrt{2\pi}}r_+\left(\frac{1}{2}\beta^2r_+^2-1\right)\exp[-i\theta_+]$	$\frac{\beta^6}{2\pi}r_+^3\exp[i\theta_+]$
$m_1=0$	$-\frac{\beta^4}{\sqrt{2\pi}}r_+\left(\frac{1}{2}\beta^2r_+^2-1\right)\exp[-i\theta_+]$	0	$\frac{\beta^6}{2\sqrt{2\pi}}r_+^3\exp[3i\theta_+]$
$m_1=+2$	$-\frac{\beta^6}{2\pi}r_+^3\exp[i\theta_+]$	$-\frac{\beta^6}{2\sqrt{2\pi}}r_+^3\exp[3i\theta_+]$	0

TABLE IV. Eigenenergy $E_{\Gamma_n^i}$ and eigenstates Γ_n^i of local Hamiltonian $\mathscr{H}_\Delta^{\rm L}$ for $d^{n=1,2,3}$ configurations. $|{\rm vac}\rangle$ is the vacuum state.

	d^1 configuration			d^2 configuration			d^3 configuration
i	1	2	3	1	2	3	1
$E_{\Gamma_n^i}$	Δ	0	Δ	$U+\Delta$	$2U+2\Delta$	$U+\Delta$	$4U+2\Delta$
$\lvert\Gamma_n^i\rangle$	$d_{xy}^\dagger\lvert{\rm vac}\rangle$	$d_{x^2+y^2}^\dagger\lvert{\rm vac}\rangle$	$d_{x^2-y^2}^\dagger\lvert{\rm vac}\rangle$	$d_{xy}^\dagger d_{x^2+y^2}^\dagger\lvert{\rm vac}\rangle$	$d_{xy}^\dagger d_{x^2-y^2}^\dagger\lvert{\rm vac}\rangle$	$d_{x^2+y^2}^\dagger d_{x^2-y^2}^\dagger\lvert{\rm vac}\rangle$	$d_{xy}^\dagger d_{x^2+y^2}^\dagger d_{x^2-y^2}^\dagger\lvert{\rm vac}\rangle$

APPENDIX C: DERIVATION OF ORBITAL SUPEREXCHANGE HAMILTONIAN $\mathscr{H}_\Delta^{\rm eff}$

To derive the effective low-energy Hamiltonian, we first diagonalize the local on-site Hamiltonian as follows:

$$\begin{aligned}\mathscr{H}_\Delta^{\rm L} &\equiv \mathscr{H}_\Delta + \mathscr{H}_{\rm I} = \Delta(d_{x^2-y^2}^\dagger d_{x^2-y^2} + d_{xy}^\dagger d_{xy}) \\ &\quad + U[(\hat{n}_{x^2-y^2}+\hat{n}_{xy})\hat{n}_{x^2+y^2} + 2\hat{n}_{x^2-y^2}\hat{n}_{xy}] \\ &= \sum_{\Gamma_n} E_{\Gamma_n^i}\lvert\Gamma_n^i\rangle\langle\Gamma_n^i\rvert,\end{aligned}$$

where Γ_n^i is the ith eigenstate of the d^n configuration with eigenenergy $E_{\Gamma_n^i}^i$. The eigenstates Γ_n^i and eigenenergies $E_{\Gamma_n^i}$ for $d^{n=1,2,3}$ configurations are listed in Table IV. In the large-U limit, the ground state of the d^2 configuration with energy $U+\Delta$ is an orbital doublet $\Gamma_2^{1,3}$ with one fermion occupying $d_{x^2+y^2}$ and the other one occupying either d_{xy} or $d_{x^2-y^2}$ orbital. Note that the doublet $\Gamma_2^{1,3}$ is well separated from the excited state Γ_2^2 by the energy gap $U+\Delta$. Therefore, in the large-U limit, it is reasonable to construct an effective model based on the doublet $\Gamma_2^{1,3}$ with the degenerate perturbation theory. For convenience, we introduce the pseudospin operators $\{\tau^+,\tau^-\}\equiv\{d_{x^2-y^2}^\dagger d_{xy}\hat{n}_{x^2+y^2}, d_{xy}^\dagger d_{x^2-y^2}\hat{n}_{x^2+y^2}\}$, which flip the states of orbital doublet. The z component of pseudospin $\boldsymbol{\tau}$ vector follows through the spin-1/2 angular-momentum algebra $\tau^z=[\tau^+,\tau^-]$. Unlike for a spin system, the charge excitation $(d^2)_i(d^2)_j \rightleftharpoons (d^3)_i(d^1)_j$, associated with the hopping process $t_{\mu\nu}d_{i\mu}^\dagger d_{j\nu}$, is directional dependent. It originates from the fact that the hopping process is anisotropic due to the spatial orientation of d orbitals. Let us first derive the superexchange interaction along $\boldsymbol{e}_1$ bonds as shown in Fig. 1(a). Employing the second-order perturbation theory [47], the matrix form of a superexchange interaction is given by

$$\begin{aligned}(J)_{kl;k'l'} = -\sum_{pq}&\frac{1}{E_{\Gamma_3^p}+E_{\Gamma_1^q}-2(U+\Delta)} \\ &\times\left\langle\begin{matrix}\Gamma_2^k & \Gamma_2^l\\ i\text{-site}&j\text{-site}\end{matrix}\middle|\sum_{\mu\nu}t_{\mu\nu}^* d_{j\nu}^\dagger d_{i\mu}\middle|\begin{matrix}\Gamma_3^p & \Gamma_1^q\\ i\text{-site}&j\text{-site}\end{matrix}\right\rangle \\ &\times\left\langle\begin{matrix}\Gamma_3^p & \Gamma_1^q\\ i\text{-site}&j\text{-site}\end{matrix}\middle|\sum_{\mu'\nu'}t_{\mu'\nu'} d_{i\mu'}^\dagger d_{j\nu'}\middle|\begin{matrix}\Gamma_2^{k'} & \Gamma_2^{l'}\\ i\text{-site}&j\text{-site}\end{matrix}\right\rangle \\ &+ i\leftrightarrow j.\end{aligned}$$

A lengthy but straightforward algebra on the summation of all bonds along the $\boldsymbol{e}_1$ vector leads to

$$\mathscr{H}_\Delta^{\boldsymbol{e}_1} = J_{\rm C}\sum_i \tau_i^z\tau_{i\pm\boldsymbol{e}_1}^z + J_{\rm H}\sum_i \boldsymbol{\tau}_i\cdot\boldsymbol{\tau}_{i\pm\boldsymbol{e}_1},$$

where

$$\begin{aligned}J_{\rm C} &= (t_{x^2-y^2,x^2-y^2}-t_{xy,xy})^2/2U, \\ J_{\rm H} &= t_{xy,xy}t_{x^2-y^2,x^2-y^2}/U.\end{aligned}$$

The hopping term $t_{xy,xy}$ ($t_{x^2-y^2,x^2-y^2}$) denotes the intraorbital hopping integral of the d_{xy} ($d_{x^2-y^2}$) orbital along the bond vector $\boldsymbol{e}_1$. Note that the bond vector $\boldsymbol{e}_1$ lies in the nodal plane of the d_{xy} orbital and thus $t_{xy,xy}$ can be labeled by π-bonding t_π. While the bonding state $t_{x^2-y^2,x^2-y^2}$ is symmetrical with respect to a π rotation about the bond vector $\boldsymbol{e}_1$ and thus is labeled by σ-bonding t_σ. Having derived the superexchange model $\mathscr{H}_\Delta^{\boldsymbol{e}_1}$ along the bond vector $\boldsymbol{e}_1$, the corresponding superexchange Hamiltonian $\mathscr{H}_\Delta^{\boldsymbol{e}_{2,3}}$ has exactly the same form with $\mathscr{H}_\Delta^{\boldsymbol{e}_1}$ if the pseudospin operators $\boldsymbol{\tau}$ are defined in the local coordinate. In the local coordinate, the local x axis is defined along a $\boldsymbol{e}_{2,3}$ bond vector. Thus, the connection between the local and global coordinates (the global x axis along the $\boldsymbol{e}_1$ bond vector) is linked by a rotation of $\theta=\frac{2\pi}{3},\frac{4\pi}{3}$ about the z axis, corresponding to the $\boldsymbol{e}_2,\boldsymbol{e}_3$ bonds, respectively. The d-orbital wave functions transform under the rotation as

$$\begin{aligned}d_{x^2-y^2} &\to \cos[2\theta]d_{x^2-y^2} - \sin[2\theta]d_{xy}, \\ d_{xy} &\to \sin[2\theta]d_{x^2-y^2} + \cos[2\theta]d_{xy}, \\ d_{x^2+y^2} &\to d_{x^2+y^2}.\end{aligned}$$

Accordingly, the pseudospin operators $\boldsymbol{\tau}$ transform as follows:

$$\begin{aligned}\tau^z &\to \sin[4\theta]\tau^x + \cos[4\theta]\tau^z, \\ \tau^x &\to \cos[4\theta]\tau^x - \sin[4\theta]\tau^z, \\ \tau^y &\to \tau^y.\end{aligned}$$

The pseudospin vector $\boldsymbol{\tau}$ is rotated by 4θ about its y axis in the pseudospin space. It is now straightforward to obtain the Hamiltonian $\mathscr{H}_\Delta^{\boldsymbol{e}_{2,3}}$ by replacing the pseudospin $\boldsymbol{\tau}$ in $\mathscr{H}_\Delta^{\boldsymbol{e}_1}$. Finally, the total superexchange Hamiltonian takes the form

$$\mathscr{H}_\Delta^{\rm eff} \equiv \sum_{i=1}^3 \mathscr{H}_\Delta^{\boldsymbol{e}_i} = J_{\rm C}\sum_{i\gamma\eta}\tau_i^\gamma\tau_{i+\eta\boldsymbol{e}_\gamma}^\gamma + J_{\rm H}\sum_{i\gamma\eta}\boldsymbol{\tau}_i\cdot\boldsymbol{\tau}_{i+\eta\boldsymbol{e}_\gamma}$$

with

$$\begin{aligned}\tau^\gamma &= \tau^z\cos[4\theta_\gamma] + \tau^x\sin[4\theta_\gamma], \\ \boldsymbol{e}_\gamma &= \hat{x}\cos\theta_\gamma + \hat{y}\sin\theta_\gamma, \\ \{\theta_1,\theta_2,\theta_3\} &= \left\{0,\frac{2\pi}{3},\frac{4\pi}{3}\right\},\quad \eta=\pm1.\end{aligned}$$

Thus, the effective Hamiltonian is described by the Heisenberg-compass model.

[1] Y. Tokura and N. Nagaosa, Science **288**, 462 (2000).

[2] S. Maekawa, T. Tohyama, S. E. Barnes, S. Ishihara, W. Koshibae, and G. Khaliullin, *Physics of Transition Metal Oxides*, Springer Series in Solid-State Sciences, Vol. 144 (Springer, Berlin, 2004).

[3] M. Imada, A. Fujimori, and Y. Tokura, Rev. Mod. Phys. **70**, 1039 (1998).

[4] A. Damascelli, Z. Hussain, and Z.-X. Shen, Rev. Mod. Phys. **75**, 473 (2003).

[5] A. P. Mackenzie and Y. Maeno, Rev. Mod. Phys. **75**, 657 (2003).

[6] N. P. Armitage, P. Fournier, and R. L. Greene, Rev. Mod. Phys. **82**, 2421 (2010).

[7] G. R. Stewart, Rev. Mod. Phys. **83**, 1589 (2011).

[8] P. Dai, Rev. Mod. Phys. **87**, 855 (2015).

[9] E. Dagotto, T. Hotta, and A. Moreo, Phys. Rep. **344**, 1 (2001).

[10] G. Khaliulli, Prog. Theor. Phys. Suppl. **160**, 155 (2005).

[11] A. M. Oleś, in *The Physics of Correlated Insulators, Metals, and Superconductors* (Forschungszentrum Jülich, Jülich, Germany, 2017).

[12] G. Jackeli and G. Khaliullin, Phys. Rev. Lett. **102**, 017205 (2009).

[13] J. Chaloupka, G. Jackeli, and G. Khaliullin, Phys. Rev. Lett. **110**, 097204 (2013).

[14] A. Banerjee *et al.*, Nat. Mater. **15**, 733 (2016).

[15] A. Banerjee *et al.*, Science **356**, 1055 (2017).

[16] S.-H. Do *et al.*, Nat. Phys. **13**, 1079 (2017).

[17] N. Janša *et al.*, Nat. Phys. **14**, 786 (2018).

[18] Y. Kasahara *et al.*, Nature **559**, 227 (2018).

[19] I. Bloch, J. Dalibard, and S. Nascimbène, Nat. Phys. **8**, 267 (2012).

[20] M. Lewenstein and W. V. Liu, Nat. Phys. **7**, 101 (2011).

[21] T. Kock, C. Hippler, A. Ewerbeck, and A. Hemmerich, J. Phys. B **49**, 042001 (2016).

[22] X. Li and W. V. Liu, Rep. Prog. Phys. **79**, 116401 (2016).

[23] A. B. Kuklov, Phys. Rev. Lett. **97**, 110405 (2006).

[24] A. Isacsson and S. M. Girvin, Phys. Rev. A **72**, 053604 (2005).

[25] W. V. Liu and C. Wu, Phys. Rev. A **74**, 013607 (2006).

[26] V. W. Scarola and S. Das Sarma, Phys. Rev. Lett. **95**, 033003 (2005).

[27] C. Wu, W. V. Liu, J. Moore, and S. Das Sarma, Phys. Rev. Lett. **97**, 190406 (2006).

[28] C. Wu, D. Bergman, L. Balents, and S. Das Sarma, Phys. Rev. Lett. **99**, 070401 (2007).

[29] E. Zhao and W. V. Liu, Phys. Rev. Lett. **100**, 160403 (2008).

[30] C. Wu, Phys. Rev. Lett. **100**, 200406 (2008).

[31] F. Pinheiro, G. M. Bruun, J.-P. Martikainen, and J. Larson, Phys. Rev. Lett. **111**, 205302 (2013).

[32] G. Wirth, M. Olschlager, and A. Hemmerich, Nat. Phys. **7**, 147 (2011).

[33] M. Ölschläger, T. Kock, G. Wirth, A. Ewerbeck, C. M. Smith, and A. Hemmerich, New J. Phys. **15**, 083041 (2013).

[34] T. Kock, M. Ölschläger, A. Ewerbeck, W.-M. Huang, L. Mathey, and A. Hemmerich, Phys. Rev. Lett. **114**, 115301 (2015).

[35] M. Ölschläger, G. Wirth, and A. Hemmerich, Phys. Rev. Lett. **106**, 015302 (2011).

[36] M. Ölschläger, G. Wirth, T. Kock, and A. Hemmerich, Phys. Rev. Lett. **108**, 075302 (2012).

[37] Y. Zhai, X. Yue, Y. Wu, X. Chen, P. Zhang, and X. Zhou, Phys. Rev. A **87**, 063638 (2013).

[38] Z. Wang, B. Yang, D. Hu, X. Chen, H. Xiong, B. Wu, and X. Zhou, Phys. Rev. A **94**, 033624 (2016).

[39] D. Jaksch and P. Zoller, Ann. Phys. (NY) **315**, 52 (2005).

[40] K. I. Petsas, A. B. Coates, and G. Grynberg, Phys. Rev. A **50**, 5173 (1994).

[41] C. Becker, P. Soltan-Panahi, J. Kronjäger, S. Dörscher, K. Bongs, and K. Sengstock, New J. Phys. **12**, 065025 (2010).

[42] J. Struck *et al.*, Science **333**, 996 (2011).

[43] J. Struck *et al.*, Nat. Phys. **9**, 738 (2013).

[44] The Wannier function $\Psi_{[n=2,m=0]}$ is defined as the s_{r^2-1} orbital in Ref. [21]. Here we defined it as the $d_{x^2+y^2}$ orbital since its orientational anisotropy is identical to that of the $d_{x^2+y^2}$ orbital in solid-state systems.

[45] E. Pavarini, in *Correlated Electrons: From Models to Materials* (Forschungszentrum Jülich, Jülich, Germany, 2012).

[46] F. D. M. Haldane, in *The Quantum Hall Effect*, 2nd ed. (Springer, New York, 1990).

[47] A. B. Kuklov and B. V. Svistunov, Phys. Rev. Lett. **90**, 100401 (2003).

[48] J. van den Brink, New J. Phys. **6**, 201 (2004).

[49] Z. Nussinov and J. van den Brink, Rev. Mod. Phys. **87**, 1 (2015).

[50] J. van den Brink, P. Horsch, F. Mack, and A. M. Oleś, Phys. Rev. B **59**, 6795 (1999).

[51] K. I. Kugel and D. I. Khomskii, Sov. Phys. Usp. **25**, 231 (1982).

[52] L. G. Marland and D. D. Betts, Phys. Rev. Lett. **43**, 1618 (1979).

[53] B. Bernu, C. Lhuillier, and L. Pierre, Phys. Rev. Lett. **69**, 2590 (1992).

[54] B. Bernu, P. Lecheminant, C. Lhuillier, and L. Pierre, Phys. Rev. B **50**, 10048 (1994).

[55] I. Bloch, J. Dalibard, and W. Zwerger, Rev. Mod. Phys. **80**, 885 (2008).

[56] M. S. Dresselhaus, G. Dresselhaus, and A. Jorio, *Group Theory: Application to the Physics of Condensed Matter* (Springer, Berlin, Heidelberg, 2008).